

Tunable electronic properties of GaS-SnS_2 heterostructure by strain and electric field

Da-Hua Ren(任达华), Qiang Li(李强), Kai Qian(钱楷), and Xing-Yi Tan(谭兴毅)

Citation: Chin. Phys. B, 2022, 31 (**4**): 047102. DOI: 10.1088/1674-1056/ac3a62
Journal homepage: http://cpb.iphy.ac.cn; http://iopscience.iop.org/cpb

What follows is a list of articles you may be interested in

Stability, electronic structure, and optical properties of lead-free perovskite monolayer $Cs_3B_2X_9$ (*B*=Sb, Bi; *X*=Cl, Br, I) and bilayer vertical heterostructure $Cs_3B_2X_9/Cs_3B_2'X_9$ (*B*,*B*'=Sb, Bi; *X*=Cl, Br, I)

Yaowen Long(龙耀文), Hong Zhang(张红), and Xinlu Cheng(程新路)
Chin. Phys. B, 2022, 31 (**2**): 027102. DOI: 10.1088/1674-1056/ac2e5f

Electronic and optical properties of 3N-doped graphdiyne/MoS_2 heterostructures tuned by biaxial strain and external electric field

Dong Wei(魏东), Yi Li(李依), Zhen Feng(冯振), Gaofu Guo(郭高甫), Yaqiang Ma(马亚强), Heng Yu(余恒), Qingqing Luo(骆晴晴), Yanan Tang(唐亚楠), and Xianqi Dai(戴宪起)
Chin. Phys. B, 2021, 30 (**11**): 117103. DOI: 10.1088/1674-1056/ac1927

Investigation of electronic, elastic, and optical properties of topological electride Ca_3Pb via first-principles calculations

Chang Sun(孙畅), Xin-Yu Cao(曹新宇), Xi-Hui Wang(王西惠), Xiao-Le Qiu(邱潇乐), Zheng-Hui Fang(方铮辉), Yu-Jie Yuan(袁宇杰), Kai Liu(刘凯), and Xiao Zhang(张晓)
Chin. Phys. B, 2021, 30 (**5**): 057104. DOI: 10.1088/1674-1056/abec38

Ab initio study of structural, electronic, thermo-elastic and optical properties of Pt_3Zr intermetallic compound

Wahiba Metiri, Khaled Cheikh
Chin. Phys. B, 2020, 29 (**4**): 047101. DOI: 10.1088/1674-1056/ab7223

Exploration of the structural and optical properties of a red-emitting phosphor $K_2TiF_6:Mn^{4+}$

Xi-Long Dou(豆喜龙), Xiao-Yu Kuang(邝小渝), Xin-Xin Xia(夏欣欣), Meng Ju(巨濛)
Chin. Phys. B, 2019, 28 (**1**): 017107. DOI: 10.1088/1674-1056/28/1/017107

Tunable electronic properties of GaS–SnS_2 heterostructure by strain and electric field

Da-Hua Ren(任达华)[1,2,†], Qiang Li(李强)[3], Kai Qian(钱楷)[3], and Xing-Yi Tan(谭兴毅)[4]

[1] *School of Information Engineering, Hubei Minzu University, Enshi* 44500, *China*
[2] *Science of Physics and Technology, Wuhan University, Wuhan* 430072, *China*
[3] *School of Advanced Materials and Mechatronic Engineering, Hubei Minzu University, Enshi* 44500, *China*
[4] *Department of Physics, Chongqing Three Gorges University, Wanzhou* 404100, *China*

(Received 9 July 2021; revised manuscript received 30 September 2021; accepted manuscript online 17 November 2021)

Vertically stacked heterostructures have received extensive attention because of their tunable electronic structures and outstanding optical properties. In this work, we study the structural, electronic, and optical properties of vertically stacked GaS–SnS_2 heterostructure under the frame of density functional theory. We find that the stacked GaS–SnS_2 heterostructure is a semiconductor with a suitable indirect band gap of 1.82 eV, exhibiting a type-II band alignment for easily separating the photo-generated carriers. The electronic properties of GaS–SnS_2 heterostructure can be effectively tuned by an external strain and electric field. The optical absorption of GaS–SnS_2 heterostructure is more enhanced than those of the GaS monolayer and SnS_2 monolayer in the visible light region. Our results suggest that the GaS–SnS_2 heterostructure is a promising candidate for the photocatalyst and photoelectronic devices in the visible light region.

Keywords: GaS–SnS_2 heterostructure, type-II band alignment, optical properties, density functional theory

PACS: 71.15.Mb, 74.78.Fk, 78.67.–n **DOI:** 10.1088/1674-1056/ac3a62

1. Introduction

Van der Waals (vdW) heterostructures can be used in unusual electronic devices because of their peculiar physical properties and excellent performances.[1] Additionally, vertically stacked heterostructures have innovative applications in electronic devices, such as ultrathin photodetectors,[2] solar cells,[3] memory devices,[4] flexible sensors, and transistors.[5,6] Specifically, two-dimensional (2D) vdW heterostructure with type-II band alignment has promising potentials in photovoltaics devices and photocatalysts[7–11] due to their fascinating electronic and optical properties. In type-II heterostructures, the photogenerated holes and electrons are spatially located in different layers. As a result, the recombination of carriers can be effectively prevented and the light energy utilization is significantly enhanced.[12] Moreover, GaS is a typical layered group III–VI compound and each layer is composed of S–Ga–Ga–S repeating units along the c axis with D_{3h} symmetry. The interlayer interactions between layers belong in weak vdW force. The GaS can be used for a promising near-blue light emitting devices because of the indirect band gap of 2.5 eV.[13] More interestingly, monolayer GaS can be easily mechanically cleavaged.[14] The photodetectors based on GaS nanosheet have higher photoresponsivity than graphene, 2D MoS_2.[15] Recent researches indicate that the vdW heterostructures based on monolayer GaS are able to exhibit type-II band alignment, such as GaS–GaSe,[16] GaS–$MoSe_2$,[17] and GaS–InS.[18]

Furthermore, tin disulfide (SnS_2) has attracted intense attention in solar energy conversion, optoelectronics, and photocatalyst because of its CdI_2-type layered structure with a sustainable band gap (2.2 eV–2.35 eV) and high electrical conductivity.[19] The SnS_2 consists of an S–Sn–S triple layer and the interlayer interaction belongs in the vdW force. The SnS_2 single-layer is synthesized by liquid exfoliation. The experimental researches indicate that the SnS_2 single-layer is of a semiconductor with a band gap of 2.29 eV and can be used in visible-light water splitting due to the high photo-conversion efficiency.[20] However, an inconvenient band edge alignment of pristine SnS_2 hinders the efficient photocatalyst from splitting water.[21] Recent efforts have demonstrated that the electronic and optical properties of SnS_2 can be greatly tailored by external means, such as doping,[22] electric field,[23] and stacking heterostructure with other 2D materials.[24]

Up to now, the combination of SnS_2 with different semiconductors, such as SnS_2–TiO_2,[24] SnS_2–g-C_3N_4,[25] SnS_2–SnO_2,[26] SnS_2–RGO,[27] and ZrS_2–SnS_2,[28] has been reported to enhance photocatalytic performance. In addition, the heterostructure based on 2D SnS_2, such as SnS_2–$BiPO_4$[29] heterostructure, are able to be formed into a type-II band structure, which shows good electronic and optical behaviors in photocatalyst and optoelectronic applications. Even though there exist a few of researches on 2D heterostructure based on 2D SnS_2, the understanding of the role and evolution of SnS_2 in the GaS–SnS_2 heterostrucutre has not been demonstrated.

Herein, we constructe a novel 2D GaS–SnS_2 heterostructure and study the structural, electronic, optical, photocalytic

[†]Corresponding author. E-mail: rdh_perfect@163.com

© 2022 Chinese Physical Society and IOP Publishing Ltd

properties. Note that 2D SnS_2, together with 2D GaS, can form a vdW heterostructure due to their similar structures and same lattice constants. Generally, it is also worth studying the superior structure and excellent properties of GaS–SnS_2 heterostructure, which could potentially provide a platform for applications in photocalyst and optoelectronic devices.

2. Computational methods

Ab initio calculations were performed within the framework of density functional theory (DFT).[30,31] as implemented in the Vienna *ab initio* simulations package (VASP).[32] Electronic exchange and correlation effects were described with the Perdew–Burke–Ernzerhof (PBE)[33] functional of generalized gradient approximation (GGA)[34] and HSE06[35] hybrid function. Electron–ion interactions were treated with the projector augmented wave (PAW) method,[36,37] with an energy cutoff being 500 eV and Brillouin zone sampling of K-mesh set to be $11 \times 11 \times 1$ for relaxation. The K-mesh points for density of states (DOS) and energy band structure calculations were assumed to be $13 \times 13 \times 1$, and the energy criterion was set to be 10^5 eV until the residual force was smaller than 10^3 eV/Å. Especially, the vacuum layer thickness is fixed at more than 25 Å to avoid spurious interactions in the neighboring images. As the long-range vdW interaction is important for holding the 2D heterostructure together, the vdW-D3 approach[38] was used to describe long-range electron correlation effects.

The optical properties of 2D GaS–SnS_2 heterostructures are described by the complex dielectric function $\varepsilon(\omega) = \varepsilon_1(\omega) + \mathrm{i}\varepsilon_2(\omega)$, where $\varepsilon_1(\omega)$ and $\varepsilon_2(\omega)$ are the real part and the imaginary part, respectively. At the same time, the imaginary part is calculated by summing up all possible transitions from the occupied to the unoccupied states, which is related to the band structure in the absorption behaviors.[39] The imaginary part is given by

$$\varepsilon_2(\hbar\omega) = \left(\frac{4\pi^2 e^2}{m\omega^2}\right) \sum_{i,j} \int_k \langle i|M|j\rangle^2 f_i\left(1 - f_i^i\right) \times \delta\left(E_{j,k} - E_{i,k} - \omega\right) \mathrm{d}^3 k, \quad (1)$$

where e, m, and ω are the charge, mass of free electron, and the frequency of incident photon, respectively. Meanwhile, M, i, j, and f_i are the dipole momentum, the index of initial state, the index of final state, and the Fermi–Dirac distribution function for ith state with wave vector $\boldsymbol{k}$, respectively. The real part $\varepsilon_1(\omega)$ is obtained from the imaginary $\varepsilon_2(\omega)$ through Kramers–Kronig relation[40,41]

$$\varepsilon_1(\omega) = 1 + \frac{2}{\pi} P \int_0^\infty \frac{\omega' \varepsilon_2(\omega') \mathrm{d}\omega'}{(\omega'^2 - \omega^2)}, \quad (2)$$

where P is the principal value. The absorption coefficient is then obtained as follows:[40,41]

$$\alpha(\omega) = \frac{\sqrt{2}\omega}{C} \left[\sqrt{\varepsilon_1^2(\omega) + \varepsilon_2^2(\omega)} - \omega_1(\omega)\right]^{1/2}. \quad (3)$$

3. Results and discussion

3.1. Stability and structures

Stacking patterns can modulate the electronic properties of the vdW heterostructures. In stacking (AA), the Sn atom is placed on the top of Ga atom, while the S atom in SnS_2 layer is situated on the top of S atom in GaS layer. In stacking (AB), the S atom in SnS_2 layer is placed on the top of Ga atom while the Sn atom is located at the hexagonal site. In stacking (AC), the Sn atom is placed on the top of S atom in GaS layer, while the S atom in SnS_2 layer is settled at the hexagonal site. In stacking (AD), the Sn atom is placed on the top of S atom in GaS layer while the S atom in SnS_2 layer lies on the top of Ga atom. We check the structural stability of these heterostructures by calculating their binding energy values, interlayer distances and thermal stabilities. Therefore, a typical stacking configuration (AA) is constructed due to the lowest adhesion energy and thermal stability. The relaxed structure is shown in Fig. 1. After relaxation, the equilibrium lattice constants of GaS monolayer ($a = b = 3.585$ Å), SnS_2 monolayer ($a = b = 3.699$ Å) and AA stacking GaS–SnS_2 heterostructure ($a = b = 3.636$ Å), calculated with GGA–PBE, are in consistence with other reported results.[14,16–19] It is clear that the hexagonal unit parameter of GaS–SnS_2 heterostructure is 3.636 Å. The lattice mismatch of GaS–SnS_2 heterostructure is 1.7%, meaning that the structure of GaS–SnS_2 heterostructure is acceptable.

To describe the vdW interaction, the interface binding energy (ΔE) of GaS–SnS_2 heterostructure is calculated to be

$$\Delta E = (E_{\mathrm{HS}} - E_{\mathrm{GaS}} - E_{\mathrm{SnS_2}})/S_0, \quad (4)$$

where ΔE refers to the interface binding energy at the interface of GaS–SnS_2 heterostructure; E_{HS}, E_{GaS}, $E_{\mathrm{SnS_2}}$, S represent respectively the total energy of heterostructure, GaS monolayer, SnS_2 monolayer, the interface areas of the heterostructure. Obviously, the interface binding energy of GaS–SnS_2 heterostructure is -27.8 meV/Å^2, demonstrating that the interaction between two layers is physically vdW force. The interface binding energy is negative, suggesting that the GaS–SnS_2 heterostructure has favorable energy during the formation. In addition, the AIMD simulation of the GaS–SnS_2 heterostructure for the most favorable stacking AA pattern is also performed to confirm the thermal stability at room temperature as can be seen in Fig. 2. Obviously, the variation of total energy of the GaS–SnS_2 heterostructure is quite small during 6800 fs, indicating that the GaS–SnS_2 heterostructure is thermally stable at room temperature.

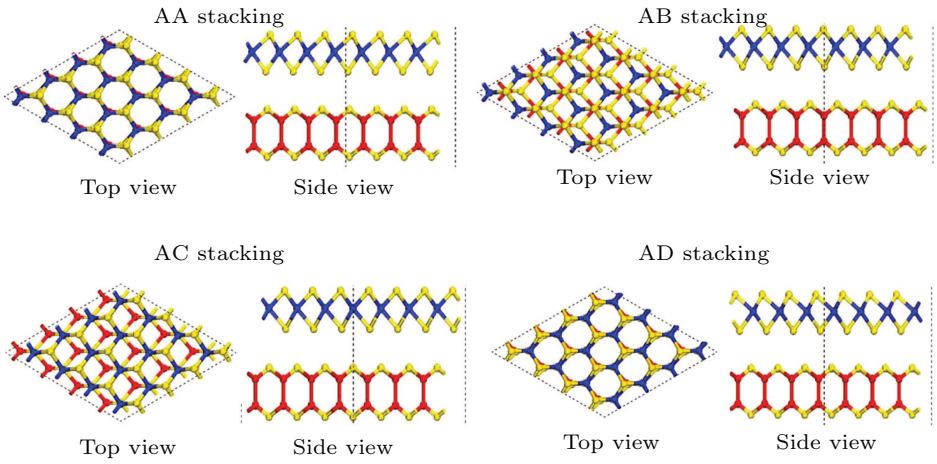


Fig. 1. Relaxed structures of four typical stacking patterns of GaS–SnS_2 heterostructure, with red, yellow, and blue spheres representing Ga, S, and Sn atoms, respectively.

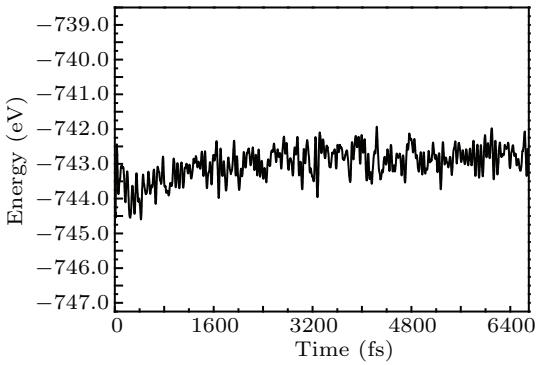


Fig. 2. Thermal stability of GaS–SnS_2 heterostructure.

As shown in Fig. 3, the optimal distance between S atom in the GaS layer and S atom in the SnS_2 layer is 3.705 Å, meaning that no bonds between S atoms are formed and this heterostructure is formed by the same magnitude order of vdW forces as typical vdW graphite.[42]

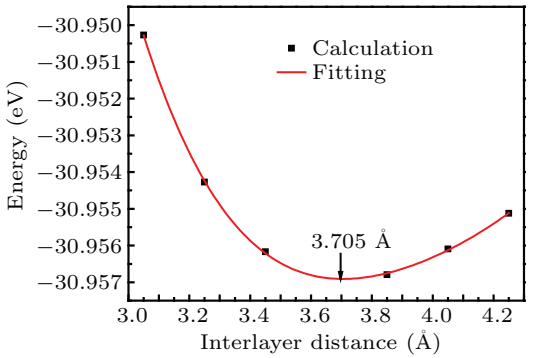


Fig. 3. Plot for the 4-th order polynomial fit interface binding energy as a function of interlayer distance of GaS–SnS_2 heterostructure.

3.2. Electronic properties

In the following, projection-resolved band structures of GaS monolayer, SnS_2 monolayer, GaS–SnS_2 heterostructure are depicted in Fig. 4. The GaS–SnS_2 heterostructure is an indirect band gap semiconductor. The valence band maximum (VBM) and the conduction band minimum (CBM) of the GaS–SnS_2 heterostructure are located at the M point and $K \rightarrow G$ of Brillouin zone (BZ). The band gap of GaS–SnS_2 heterostructure is 1.82 eV from the HSE06 calculation, smaller than those of both individual GaS (3.19 eV) monolayer and individual SnS_2 (2.31 eV) monolayer, which accord well with the theoretical values of GaS (3.29 eV),[15] SnS_2 (2.39 eV).[43] Specially, GaS–SnS_2 heterostructure has a type-II band alignment, which is beneficial to separating the photogenerated holes and electrons in different layers, preventing the carriers from being recombined, and enhancing the light energy utilization. Therefore, the band gap of the GaS–SnS_2 heterostructure can be significantly changed by vertically stacking the heterostructure, which can provide a good opportunity to work on band engineering and photoelectronic device designs.

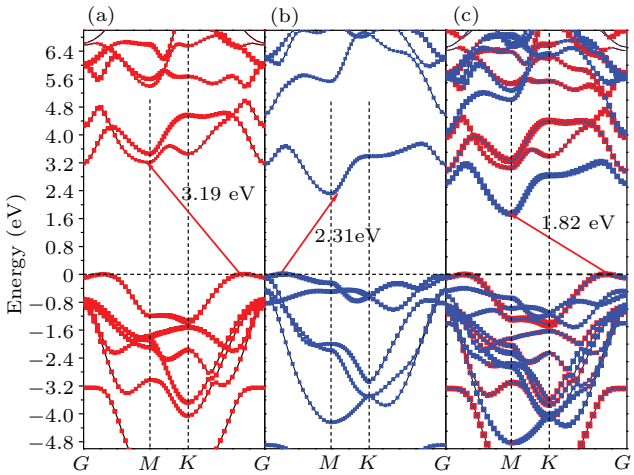


Fig. 4. Projection-resolved band structure of (a) GaS monolayer, (b) SnS_2 monolayer, and (c) GaS–SnS_2 heterostructure, with red and blue lines denoting contributions from GaS and SnS_2 layers, respectively.

As reflected in the projection-resolved band structure, the band gap of GaS monolayer decreases due to the downshift of CBM at M point as well as the upshift of VBM at $K \rightarrow G$ point. The contribution of VBM of GaS–SnS_2 heterostructure is GaS layer and that of CBM is SnS_2 layer, in which the red and blue lines present the DOS of GaS and SnS_2 layer in GaS–SnS_2 heterostructure, respectively, in Fig. 5. Obviously,

in the GaS–SnS_2 heterostructure, the VBM and CBM are respectively confined in GaS and SnS_2 layer, respectively, indicating that the GaS–SnS_2 heterostructure has a type-II band alignment.

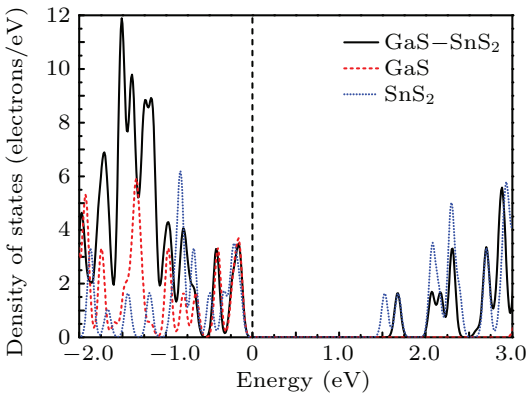


Fig. 5. Projected density of states (PDOS) of GaS monolayer, SnS_2 monolayer, GaS–SnS_2 heterostructure, where Fermi level is set to zero as indicated by the black dashed line.

3.3. Effect of external electric field and biaxial strain on band gap of GaS–SnS_2 heterostructure

External electric field is extensively considered as an efficient strategy to expand the semiconductors with desirable band gap into photoelectronic devices. Therefore, it is extremely important that an external electric field (E_{ext}) be applied to changing the band gap of GaS–SnS_2 heterostructure as depicted in Fig. 6. The band gap of GaS–SnS_2 heterostructure, which remains indirect semiconductor, changes a lot in the E_{ext} range from −0.1 V/Å to 0.1 V/Å. Note that the electric field direction from the bottom (GaS layer) to the top (SnS_2 layer) is the positive Z direction of E_{ext}, perpendicular to the interface. The band gap decreases from −0.1 V/Å to 0.1 V/Å, which accelerates electrons (holes) from the conduction band-CB (valence band-VB) of the SnS_2 (GaS) layer to the CB (VB) of the GaS (SnS_2) layer as shown in Fig. 6(b).

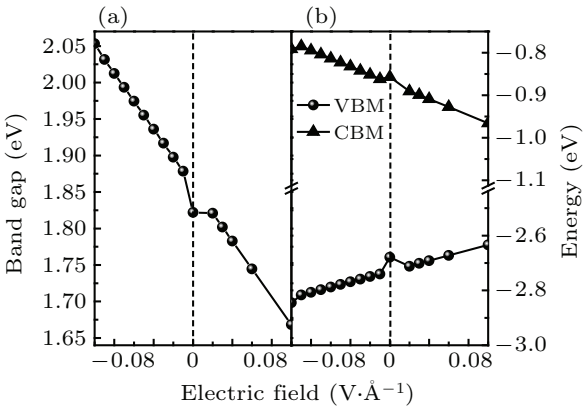


Fig. 6. Variation of (a) band gap and (b) band alignment of GaS–SnS_2 heterostructure with external electric field.

Biaxial strain is effectively able to tailor the electronic performance of heterostructure. Here, the effect of biaxial strain from −8% to 10% on the electronic property of GaS–SnS_2 heterostructure is discussed, namely the corresponding lattice parameter of the heterostrucutre unit cell is effectively modified. Fortunately, the structure of the heterostructure under biaxial strain is successfully relaxed and has the hexagonal lattice symmetry according to the same state of the irreducible Brillouin zone. The change of the band gap under biaxial strain is shown in Fig. 7. As the compress strain increases from −4% to −8%, the band gap first decreases, for the VBM increases more rapidly than the CBM. And the compress strain increases from 0 to −4%, the band gap then increases due to the more fast-growing CBM. Meanwhile, the band gap decreases monotonically when the tensile strain increases from 0 to 10% due to the CBM moving more speedily down to fermi level than the VBM.

Although the outermost two S layers in the GaS–SnS_2 heterostructure have the same electronegativity, the sixth Sn layer on the SnS_2 side has greater electronegativity (2.44 e) than the second Ga layer on the GaS side (2.14 e). Therefore, the electrons at the interface are depleted on the GaS side but accumulated on the SnS_2 side, forming a built-in electric field from GaS layer to SnS_2 layer. The smaller charge transfer at the interface leads to the weaker interaction between Sn and Ga atoms.

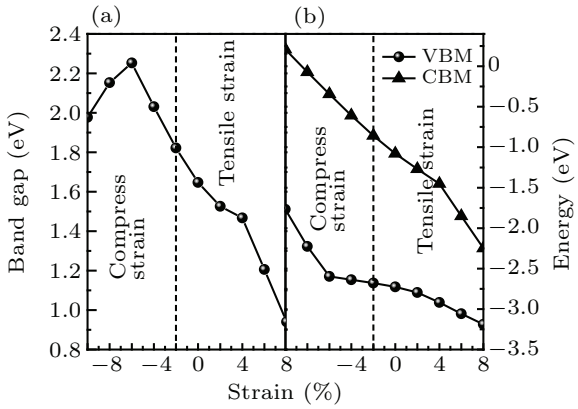


Fig. 7. Variation of (a) band gap and (b) band alignment with biaxial strain of GaS–SnS_2 heterostructure.

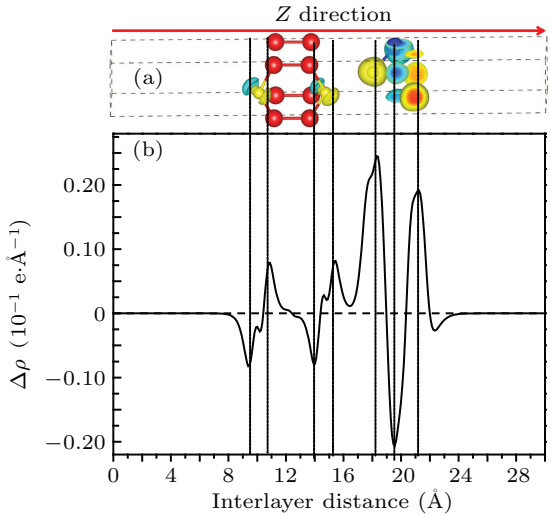


Fig. 8. (a) Charge density difference and (b) planar-averaged charge density difference of GaS–SnS_2 heterostructure along Z direction.

The planar-averaged charge density difference along the Z direction is described as $\Delta\rho = \rho_{GaS-SnS_2} - \rho_{GaS} - \rho_{SnS_2}$, where, $\rho_{GaS-SnS_2}$, ρ_{GaS}, ρ_{SnS_2} are the planar-averaged charge densities of GaS–SnS_2 heterostructure, GaS monolayer, and SnS_2 monolayer. As shown in Fig. 8, the positive value and the negative value represent the charge accumulation and the charge depletion, respectively. Both electrons and holes under built-in electric field move towards the opposite directions, which can accelerate the separation of photo-generated electrons or holes to improve photocatalytic activity.

3.4. Photocatalyst and absorption behaviors

The absorption coefficient of GaS–SnS_2 heterostructure is calculated, and the results are shown in Fig. 9(a). It is clear that the first peak in the absorption spectrum of GaS–SnS_2 heterostructure is locates at 2.25 eV, which is mainly contributed by the SnS_2 layer. The absorption behavior of GaS–SnS_2 heterostructure is more improved than that of the individual GaS monlayer and SnS_2 monolayer. The absorption spectrum of GaS–SnS_2 heterostructure covers the visible light, which makes it well suitable for the application of optoelectronic devices in visible light region.

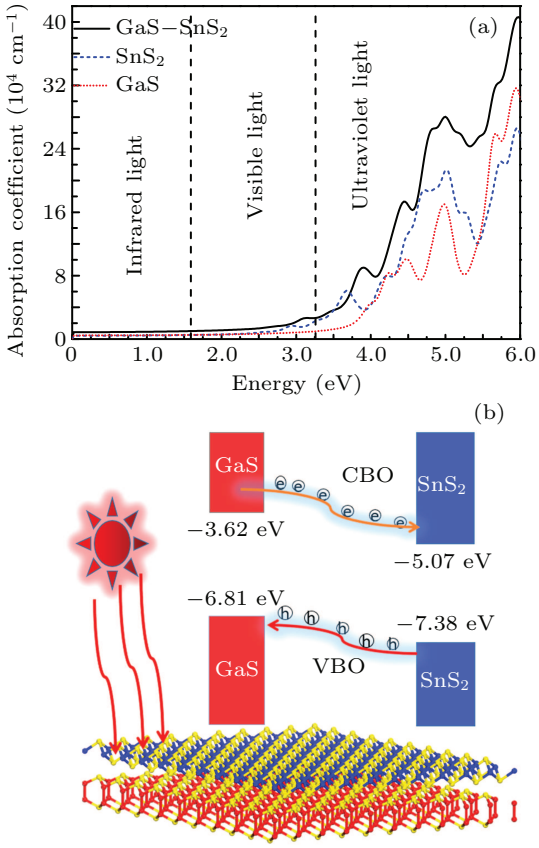


Fig. 9. (a) Absorption spectra of GaS–SnS_2 heterostructure and (b) schematic migrating carrier.

A schematic plot to depict the dynamic process of photogenerated carrier at the GaS–SnS_2 interface is shown in Fig. 9(b). In the GaS–SnS_2 heterostructure, the photogenerated electrons of the GaS layer start to transfer to the SnS_2 layer in the conduction band, which are motivated by the conduction band offset (CBO) (1.45 eV). Meanwhile, the photogenerated holes move from the valence band of the SnS_2 layer into the GaS layer, which are driven by a large valence band offset (VBO) (0.57 eV). Hence, the GaS–SnS_2 heterostructure, exhibiting a type-II band alignment, can be utilized as a photocatalyst.

As is well known, the lifetime of photogenerated carriers is significantly influenced by the build-in electric field. Hence, build-in electric field induced by ground state charge transfer are investigated based on bader charge analysis.[44] The charge transferring from the GaS layer to the SnS_2 layer is 0.938 e, leading to an electric field from the GaS layer to the SnS_2 layer. This electric field will promote interlayer charge transfer and prohibit carrier recombination, favoring a good light harvesting efficiency.

4. Conclusions

In this work, the electronic and optical properties of GaS–SnS_2 heterostructure have been investigated with density functional theory. It is found that the hexagonal GaS–SnS_2 heterostructure is a stable semiconductor with a suitable indirect band gap. Interestingly, the GaS–SnS_2 heterostructure has a type-II band alignment, which is beneficial to photocatalyst. In the GaS–SnS_2 heterostructure, the charge transferring from the GaS layer to the SnS_2 layer is 0.938 e based on bader charge analysis, forming a build-in electric field for charge separation. The absorption behavior of GaS–SnS_2 heterostructure is enhanced in comparison with that of the individual GaS monlayer and SnS_2 monolayer, indicating that the GaS–SnS_2 heterostructure is very efficient at absorbing the visible light to expand the application into photocatalyst and opto-electronic devices.

Acknowledgements

Project supported by the National Natural Science Foundation of China (Grant No. 1186040026), the Incubation Project for High-Level Scientific Research Achievements of Hubei Minzu University, China (Grant No. 4205009), and the Fund of the Educational Commission of Hubei Province, China (Grant No. T201914).

References

[1] Geim A and Grigorieva I 2013 *Nature* **499** 419
[2] Massicotte M, Schmidt P, Vialla F, Schödler K G, Reserbat P A, Watanabe K, Taniguchi T, Tielrooij K J and Koppens F H L 2015 *Nat. Nanotechnol.* **11** 42
[3] Lee C H, Lee G H, van der Zande A M, Chen W, Li Y, Han M, Cui X, Arefe G, Nuckolls C, Heinz T F, Guo J, Hone J and Kim P 2014 *Nat. Nanotechnol.* **9** 676
[4] Britnell L, Gorbachev R V, Jalil R, Belle B D, Schedin F, Mishchenko A, Georgiou T, Katsnelson M I, Eaves L, Morozov S V, Peres N M R, Leist J, Geim A K, Novoselov K S and Ponomarenko L A 2012 *Science* **335** 947

[5] Wang H, Yuan H, Sae H S, Li Y and Cui Y 2015 *Chem. Soc. Rev.* **44** 2664

[6] Lu N, Guo H, Li L, Dai J, Wang L, Mei W N, Wu X and Zeng X C 2014 *Nanoscale* **6** 2879

[7] Jiao Z Y, Wang Y R, Guo Y L and Ma S H 2021 *Chin. Phys. B* **30** 077304

[8] Peng C S, Zhou Y D, Zhang S S and Zhao Z Y 2021 *Chin. Phys. B* **30** 017101

[9] 9. Sun Y Q, Zhang J C, Cheng F M, Ning C, Zhuo N, Zhai S Q, Liu F Q, Liu J Q, Liu S M and Wang Z G 2021 *Chin. Phys. B* **30** 034211

[10] Wong J, Jariwala D, Tagliabue G, Tat K, Davoyan A R, Sherrott M C and Atwater H A 2017 *ACS Nano* **11** 7230

[11] Ren D H, Tan X Y, Zhang T and Zhang Y 2019 *Chin. Phys. B* **28** 086104

[12] Peng B, Yu G, Liu X, Liu B, Liang X, Bi L, Deng L, Sum T C and Loh K P 2016 *2D Mater.* **3** 025020

[13] Genut M, Margulis L, Hodes G and Tenne R 1992 *Thin Solid Films* **217** 97

[14] Late D J, Liu B, Matte H S S R, Rao C N R and Dravid V P 2012 *Adv. Funct. Mater.* **22** 1894

[15] Hu P A, Wang L F, Yoon M, Zhang J, Feng W, Wang X N, Wen Z Z, Idrobo J C, Miyamoto Y, Geohegan D B and Xiao K 2013 *Nano Lett.* **13** 1649

[16] Wei W, Dai Y, Niu C W, Li X, Ma Y D and Huang B B 2015 *J. Mater. Chem. C* **3** 11548

[17] Pham K D, Phuc H V, Hieu N N, Hoi B D and Nguyen C V 2018 *AIP Adv.* **8** 075207

[18] Rahman A U, Morbec J M, Rahman G and Kratzer P 2018 *Phys. Rev. Mater.* **2** 094002

[19] Huang P C, Shen Y M, Brahma S, Shaikh M O, Huang J L and Wang S C 2017 *Catalysts* **7** 252

[20] Sun Y F, Cheng H, Gao S, Sun Z H, Liu Q H, Liu Q, Lei F C, Yao T, He J F, Wei S Q and Xie Y 2012 *Angew. Chem. Int. Ed.* **51** 8727

[21] Lin J, Liu Y, Liu Y, Huang C, Liu W, Mi X, Fan D, Fan F, Lu H and Chen X 2019 *Chem. Sus. Chem.* **12** 961

[22] Shown I, Samireddi S, Chang Y C, Putikam R, Chang P H, Sabbah A, Fu F Y, Chen W F, Wu C I, Yu T Y, Chung P W, Lin M C, Chen L C and Chen K H 2018 *Nat. Commun.* **9** 169

[23] Ding Y and Wang Y 2013 *Appl. Phys. Lett.* **103** 043114

[24] Sun L Q, Zhao Z C, Li S, Su Y P, Huang L, Shao N N, Liu F, Bu Y B, Zhang H J and Zhang Z T 2019 *ACS Appl. Nano Mater.* **2** 2144

[25] Di T, Zhu B, Cheng B, Yu J and Xu J 2017 *J. Catal.* **352** 532

[26] Zhang Y C, Yao L, Zhang G, Dionysiou D D, Li J and Du X 2014 *Appl. Catal. B* **144** 730

[27] An X, Yu J C and Tang J 2014 *J. Mater. Chem. A* **2** 1000

[28] Wang J N, Huang Y H, Ma F, Zhang J M, Wei X M and Zhu G Q 2020 *J. Alloys Compd.* **849** 156627

[29] Chou X Y, Ye J, Cui M M, He Y Z and Li Y D 2020 *Mater. Chem. Phys.* **240** 122241

[30] Hohenberg P and Kohn W 1964 *Phys. Rev.* **136** B864

[31] Tong B Y and Sham L J 1966 *Phys. Rev.* **144** 1

[32] Kresse G and Hafner J 1993 *Phys. Rev. B* **47** 558

[33] Perdew J P, Burke K and Ernzerhof M 1996 *Phys. Rev. Lett.* **77** 3865

[34] Burke K, Perdew J P and Ernzerhof M 1997 *Int. J. Quantum Chem.* **61** 287

[35] Heyd J and Scuseria G E 2003 *J. Chem. Phys.* **118** 8207

[36] Kresse G and Joubert D 1999 *Phys. Rev. B* **59** 1758

[37] Blöchl P E 1994 *Phys. Rev. B* **50** 17953

[38] Grimme S, Antony J, Ehrlich S and Krieg H 2010 *J. Chem. Phys.* **132** 154104

[39] Gajdoš M, Hummer K, Kresse G, Furthmüller J and Bechstedt F 2006 *Phys. Rev. B* **73** 045112

[40] Adler S L 1962 *Phys. Rev.* **126** 413

[41] Komsa H and Krasheninnikov A V 2013 *Phys. Rev. B* **88** 085318

[42] Chen X, Tian F, Persson C, Duan W and Chen N X 2013 *Sci. Rep.* **3** 3046

[43] Wang V, Xu N, Liu J C, Tang G and Geng W T 2021 *Comput. Phys. Commun.* **267** 108033

[44] Bader R F W 1990 *Atoms in Molecules (A Quantum Theory)* (Oxford: Oxford University Press)